

Cite this: *Catal. Sci. Technol.*, 2018, 8, 2835

Origin of ligand effects on reactivities of pincer-Pd catalyzed hydrocarboxylation of allenes and alkenes with formate salts: a computational study†

Xiangying Lv,^a Fang Huang,^{iD} Yan-Bo Wu^{iD} and Gang Lu^{iD}*^d

The origin of ligand effects on pincer-Pd catalyzed hydrocarboxylation of allenes and alkenes was investigated using density functional theory (DFT) calculations. The computations reveal that the CO₂ insertion into allylpalladium and benzylpalladium intermediates is the rate-determining step for both allene and alkene substrates. Distortion/interaction analysis indicates that CO₂ insertion into the benzylpalladium intermediate *via* a 3-membered transition state has larger distortion energy than that of CO₂ reacting with the allylpalladium intermediate through a 6-membered transition state. The linear relationships between the distortion energy and the activation energy are applicable for a series of *PGeP*-pincer ligands with different *P*-bound R substituents.

Received 26th February 2018,
Accepted 24th April 2018

DOI: 10.1039/c8cy00405f

rsc.li/catalysis

1. Introduction

The use of renewable chemical feedstocks for making value-added fine chemicals is of great importance in the development of green synthesis.^{1–3} In this regard, the cheap and abundant formate salt, easily obtained from CO₂ hydrogenation^{4–10} and biomass transformations,^{11–15} has great potential as a renewable C1 resource. Instead of only acting as a reductant,^{16–18} formate salt is increasingly used as a C1 unit to form carbon-carbon bonds *via* transition metal catalysis.^{19–26} Recently, the Iwasawa group developed an efficient strategy that utilizes formate salt as a CO₂ and hydride source to fulfill hydrocarboxylation of allenes and alkenes based on pincer palladium catalysts (Scheme 1).^{27,28} In contrast to direct carboxylation using CO₂ which often uses stoichiometric amounts of reactive metallic reagents,^{29–33} this hydrocarboxylation with formate salt is quite promising due to its metallic reductant-free and atom-economical process. Furthermore, together with the pro-

cess of CO₂ hydrogenation to formate salt or formic acid,^{4–10} reactions utilizing formate salt provide an alternative protocol for CO₂ utilization in organic transformations.

In the reactions shown in Scheme 1, the *PGeP*-pincer Pd catalysts **cat1** and **cat2** with different *P*-bound R substituents were employed and show different reactivities in allene and alkene hydrocarboxylation reactions. With **cat1**, allene **1a** can be effectively hydrocarboxylated to form the carboxylic acid **3a**. In contrast, **cat1** is ineffective in reactions involving alkene **1b**. More interestingly, changing **cat1** with Ph substituents on phosphorus arms to **cat2** with Et substituents can significantly promote the reaction of alkene **1b**. Previous mechanistic studies often focused on the effects of X and the metal in *PXP*-pincer metal complexes,^{34–38} and the effect of *P*-bound R substituents on reactivity is unexplored with computations in this reaction.

The general mechanism is shown in Scheme 2. The active catalyst palladium formate (**I**) is generated *via* ligand

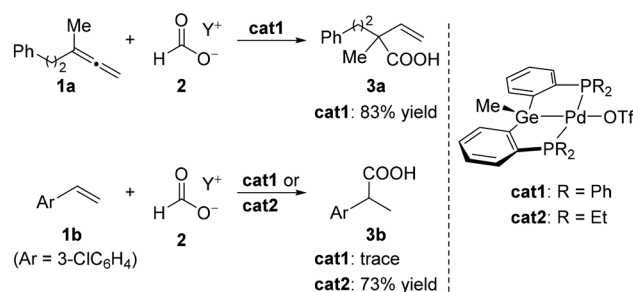
^a Key Laboratory for Yellow River and Huai River Water Environment and Pollution Control, Ministry of Education, Henan Key Laboratory for Environmental Pollution Control, School of Environment, Henan Normal University, Xinxiang, Henan 453007, P. R. China

^b College of Chemistry, Chemical Engineering and Materials Science, Shandong Normal University, Jinan 250014, P. R. China

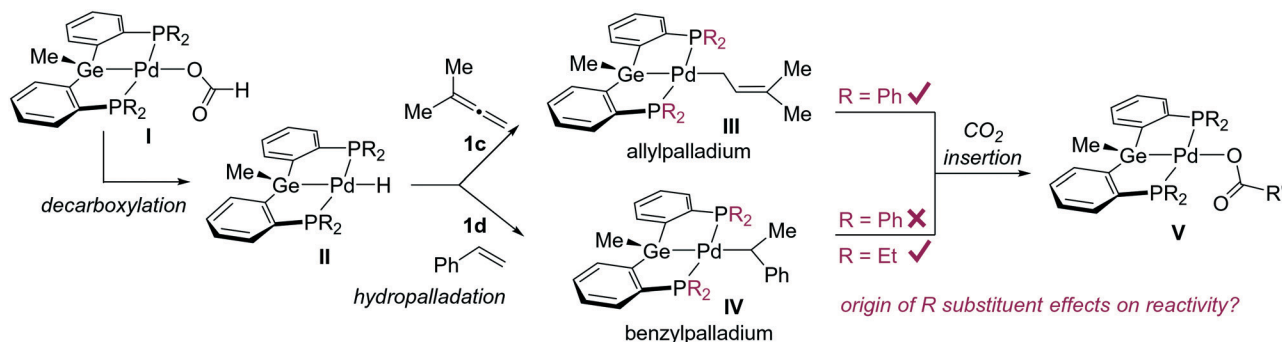
^c Key Lab for Materials of Energy Conversion and Storage of Shanxi Province and Key Lab of Chemical Biology and Molecular Engineering of Ministry of Education, Institute of Molecular Science, Shanxi University, Taiyuan, Shanxi, 030006, P. R. China

^d Department of Chemistry, University of Pittsburgh, Pittsburgh, PA, USA.
E-mail: gal40@pitt.edu

† Electronic supplementary information (ESI) available: Additional discussions of computational results; Cartesian coordinates and energies of the optimized structures. See DOI: 10.1039/c8cy00405f



Scheme 1 *PGeP*-pincer Pd catalyzed hydrocarboxylation of allenes and alkenes with formate salt. See ref. 27 and 28 for detailed experimental conditions and procedures.



Scheme 2 Proposed mechanism for *PGeP*-pincer Pd catalyzed hydrocarboxylation of allenes and alkenes.

exchange of Pd precursors with excess formate salts, which is followed by a decarboxylation process to give palladium hydride (**II**)³⁹ and release CO₂. The subsequent hydro-palladations of allene **1c** and styrene **1d** furnish allylpalladium (**III**) and benzylpalladium (**IV**) intermediates, respectively. Based on the previous computational studies of transition metal-catalyzed CO₂ functionalizations by our^{40,41} and other groups,^{42–48} it is hypothesized that CO₂ insertion into these Pd–C(allyl/benzyl) bonds may control the reactivity. However, what dominates the reactivity toward different Pd–C intermediates (allylpalladium *vs.* benzylpalladium) and how variations in the substitution patterns on the ligand framework influence the reactivity (R = Ph *vs.* R = Et) remain unclear. Here, we describe the first computational study to identify the origin of ligand effects on reactivity by way of distortion/interaction analysis⁴⁹ in this catalytic system.

2. Computational methods

All calculations were performed with Gaussian 09.⁵⁰ In geometry optimizations, the B3LYP density functional and a mixed basis set of LANL2DZ for Pd and 6-31G(d) for other atoms were used. All minima have zero imaginary frequencies and all transition states have only one imaginary frequency. Single-point energies were calculated using the M06L functional^{51,52} and a mixed basis set of SDD for Pd and 6-311+G(d,p) for other atoms. Solvation energy corrections were calculated using the SMD model.⁵³ The computed activation free energies for key transition states using several popular functionals show good consistency (see Table S1 in the ESI† for details). DMF was used as the solvent in the calculations. For the distortion/interaction analysis,⁴⁹ fragment distortion energies were computed at the M06L/SDD-6-311+G(d,p) level in the gas phase using the B3LYP/LANL2DZ-6-31G(d) optimized geometries. The 3D structures of molecules were generated using CYLview.⁵⁴

3. Results and discussion

We first studied the energy profile of the hydrocarboxylation of allene **1c** catalyzed by a *PGeP*-pincer Pd complex with Ph substituents on the P arms (Fig. 1; to simplify the calcula-

tions, 3-methyl-1,2-butadiene **1c** and styrene **1d** were used to model the substrates in the experiment). Starting from palladium formate **4**, a reversible decarboxylation process occurs with a small barrier (5-TS, $\Delta G^\ddagger = 11.1$ kcal mol⁻¹). Due to the steric effect, in the hydro-palladation transition states, the attack of Pd on the unsubstituted terminal carbon atom of allene **1c** (7-TS, $\Delta G^\ddagger = 14.0$ kcal mol⁻¹ with respect to **6**) is much more favorable than its reaction with the dimethyl-substituted carbon atom (9-TS, $\Delta G^\ddagger = 21.3$ kcal mol⁻¹ with respect to **6**). The formation of the allylpalladium intermediate **8** is highly exothermic by 22.4 kcal mol⁻¹. The Pd-allyl **8** adopts an η^1 conformation because the rigidity of the pincer ligand framework disfavors the η^3 -allyl complex. The subsequent CO₂ insertion into the Pd-allyl intermediate requires a barrier of 21.6 kcal mol⁻¹ (**11-TS**), representing the rate-determining step in the overall catalytic cycle. **11-TS** bears a pseudo-6-membered ring, which is good for CO₂ intake without inducing considerable steric clashes. In contrast, the 3-membered transition state of CO₂ insertion (**13-TS**, $\Delta G^\ddagger = 35.8$ kcal mol⁻¹ with respect to **10**) is highly disfavored due to the substantial steric congestion around the crowded Pd center.

To investigate the origin of the difference in reactivity between allene and styrene substrates, we then computed the reaction pathways for styrene hydrocarboxylation with **cat1**. The overall energy profile is described in Fig. S1†. Likewise, the CO₂ insertion into the benzylpalladium intermediate is the rate-determining step. The transition state **14-TS** is shown in Fig. 2. The computed high barrier of **14-TS** ($\Delta G^\ddagger = 34.8$ kcal mol⁻¹ with respect to the corresponding benzylpalladium intermediate) is in line with the experimental observation that a Pd catalyst ligated by a Ph-substituted *PGeP*-pincer ligand is ineffective for alkene substrates.²⁸ Similar to the disfavored **13-TS**, the 3-membered transition state **14-TS** may also have severe steric repulsions. To further identify the origin of the difference in activation free energies between **11-TS** for allenes and **14-TS** for alkenes, we performed a distortion/interaction analysis.⁴⁹ The distortion energy refers to the energy required to deform the reactants into their transition state geometries. The interaction energy includes both stabilizing interactions (such as electrostatic and orbital interactions) and destabilizing steric repulsion.

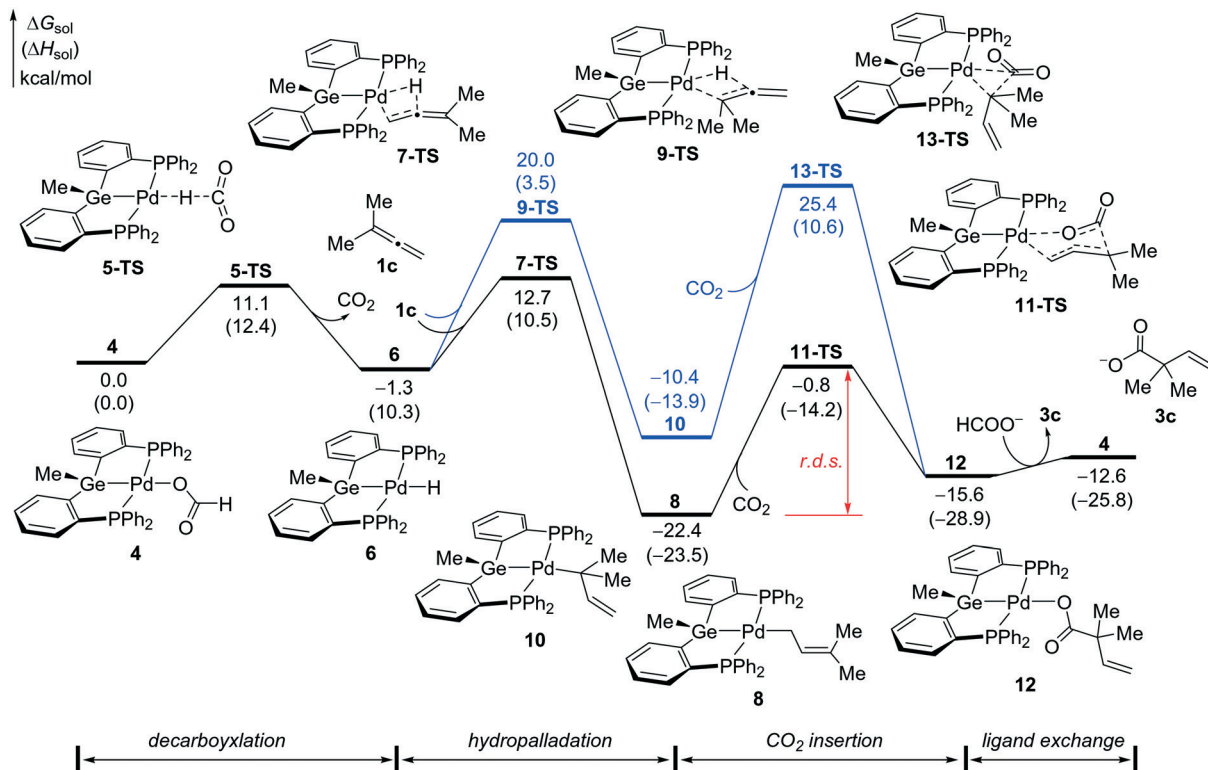


Fig. 1 Energy profile of *PGeP*-pincer Pd catalyzed hydrocarboxylation of allene **1c**. Energies are calculated with respect to the Pd formate **4**.

In Fig. 2, $\Delta E_{\text{dist}}(\text{Pd})$ is the energy required to distort the Pd-allyl or Pd-benzyl complex supported by the Ph-

substituted *PGeP*-pincer ligand into its transition state geometry. $\Delta E_{\text{dist}}(\text{CO}_2)$ is the energy used to deform CO₂ into its

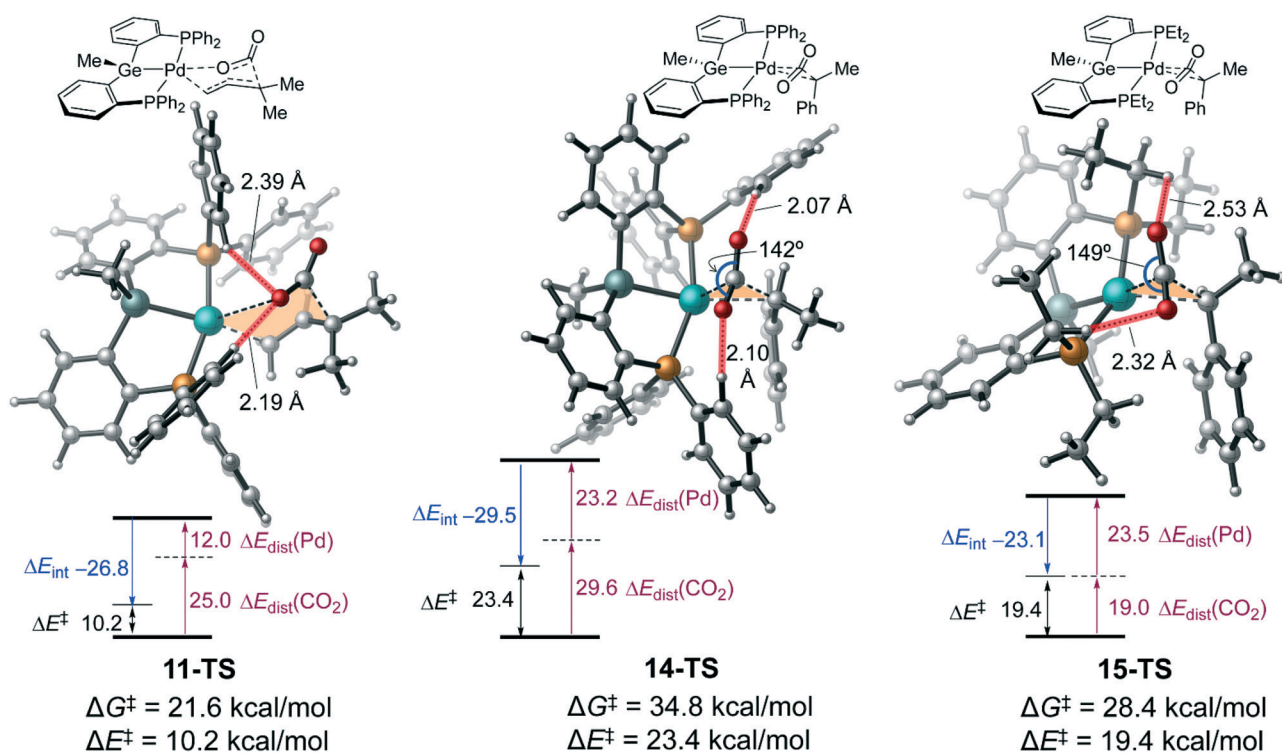


Fig. 2 Optimized geometries of CO₂ insertion transition states with allylpalladium and benzylpalladium intermediates and the distortion/interaction analysis for these transition states (energies are given in kcal mol⁻¹).

transition state geometry. The interaction energy between the distorted Pd-allyl or Pd-benzyl complex and CO₂ is denoted as ΔE_{int} . The activation energy, ΔE^\ddagger , is the sum of $\Delta E_{\text{dist}}(\text{Pd})$, $\Delta E_{\text{dist}}(\text{CO}_2)$ and ΔE_{int} .

For 11-TS and 14-TS, the distortion/interaction analysis reveals that the 13.2 kcal mol⁻¹ difference in ΔE^\ddagger can be attributed to the difference in the total distortion energies ($\Delta E_{\text{dist}}(\text{Pd}) + \Delta E_{\text{dist}}(\text{CO}_2)$). The interaction energy (ΔE_{int}) shows negative contribution to the difference in activation energy (see details in Fig. S2†). Both benzylpalladium and CO₂ in 14-TS are more distorted than those in 11-TS (11.2 kcal mol⁻¹ difference in $\Delta E_{\text{dist}}(\text{Pd})$ and 4.6 kcal mol⁻¹ difference in $\Delta E_{\text{dist}}(\text{CO}_2)$). This is mostly caused by the difference in the transition state geometries, the 3-membered transition state of 14-TS leading to more repulsive proximal contacts between CO₂ and benzylpalladium than those between CO₂ and allylpalladium in the 6-membered transition state of 11-TS. This is clearly evidenced by the relatively shorter O...H distances (2.07 and 2.10 Å) in 14-TS compared to those (2.19 and 2.39 Å) in 11-TS.⁵⁵

We further studied whether the replacement of Ph substituents with Et substituents on the *PGeP*-pincer ligand could promote the reaction with styrene. 15-TS shown in Fig. 2 is the transition state of CO₂ insertion into benzylpalladium ligated by the Et-substituted *PGeP*-pincer ligand (cat2 in Scheme 1). The computed activation free energy of 15-TS is 28.4 kcal mol⁻¹, which is 6.4 kcal mol⁻¹ lower than that of 14-TS. This is consistent with the experimentally observed efficiency of cat2.²⁸ The distortion/interaction analysis indicates that the total distortion energy in 15-TS (42.5 kcal mol⁻¹) is indeed smaller than that in 14-TS (52.8 kcal mol⁻¹), which is also supported by the longer O...H distances (2.32 Å and 2.53 Å) in 15-TS compared to those in 14-TS (Fig. 2). Although the *PGeP*-pincer ligands possess different substituents, the distortion energies of benzylpalladium ($\Delta E_{\text{dist}}(\text{Pd})$) in 14-TS and 15-TS are almost identical. In contrast, the energy expenditures required to bend CO₂ in these two transition states are significantly different, as evidenced by the different angles of $\angle\text{OCO}$ (149° in 15-TS vs. 142° in 14-TS). This makes the major contribution for the difference in activation energies between 14-TS and 15-TS.⁵⁵

Taken together, the critical effect of the *P*-bound R substituents of pincer ligands on reactivity is mostly ascribed to the steric repulsion between CO₂ and the ligands, which leads to considerable distortions of these fragments, thus affecting the CO₂ insertion reactivity.

To investigate whether the effect of distortion on reactivity is a general trend with a broader range of pincer ligands, we employed the distortion/interaction analysis to study the relationship between ΔE_{dist} and ΔE^\ddagger in CO₂ insertions with Pd-C(allyl/benzyl) intermediates ligated by *PGeP*-pincer ligands with different *P*-bound R substituents (R = Ph, Me, Et, ⁱPr, Cy, ^tBu, Fig. 3). Excellent linear correlations were observed for these ligands.⁵⁶ This indicates that the reactivity of CO₂ insertion is controlled by the total distortion energy of CO₂ and Pd-allyl/Pd-benzyl complexes.⁵⁷

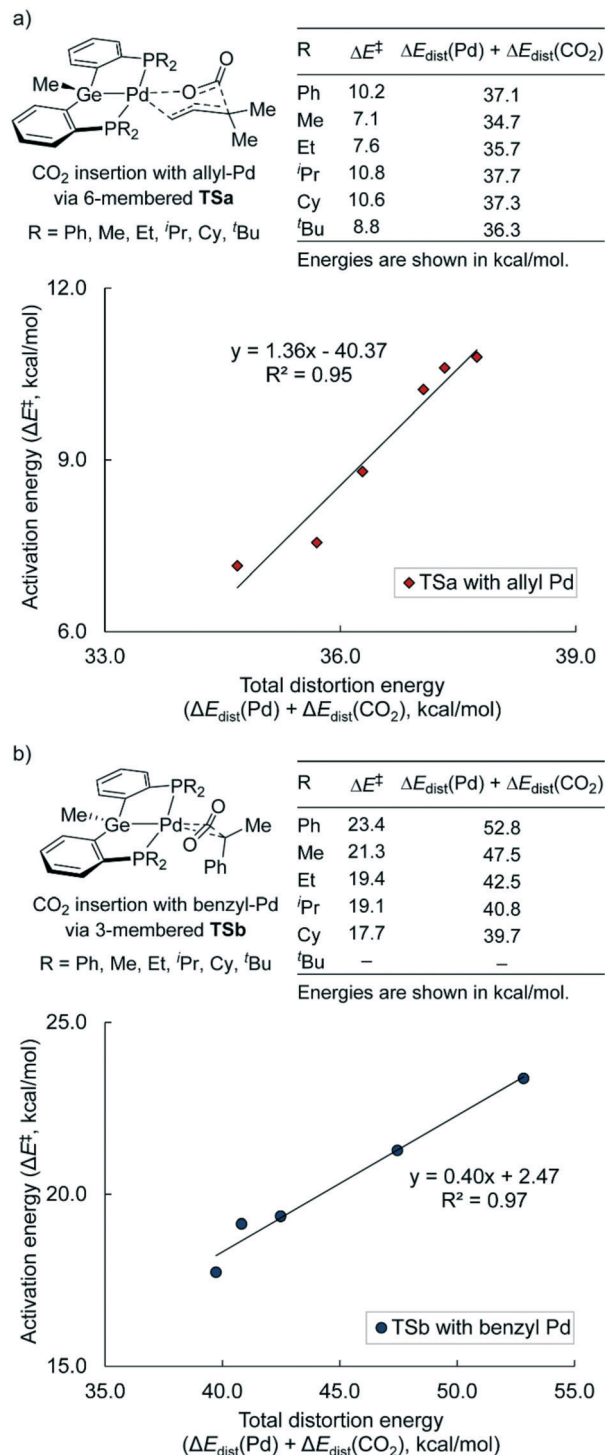


Fig. 3 Linear correlation between total distortion energy (ΔE_{dist}) and activation energy (ΔE^\ddagger) in CO₂ insertion transition states. a) The reaction of CO₂ with allylpalladium intermediates; b) the reaction of CO₂ with benzylpalladium intermediates.

As can be seen from Fig. 3, the energy variations in the total distortion energy (ΔE_{dist}) are quite different for the allylpalladium intermediate (ca. 3 kcal mol⁻¹) and the benzylpalladium intermediate (ca. 13 kcal mol⁻¹). This suggests the *P*-bound R substituents have different influences on the

reactivity of CO₂ insertion with Pd-allyl and Pd-benzyl species. This difference can be rationalized in terms of different transition state geometries. Compared to the 6-membered transition state TS_a, the 3-membered transition state TS_b forces CO₂ closer to the Pd center. Therefore, the R substituents on the P arms of pincer ligands can have a more significant influence on the distortion energy and activation energy in reactions of CO₂ with benzylpalladium intermediates.

4. Conclusions

In summary, we performed DFT calculations to investigate the origin of the effects of substituents in PGeP-pincer ligands on Pd-catalyzed hydrocarboxylation of allenes and alkenes with formate salts. The computed mechanism indicates that the CO₂ insertion is the rate-determining step for both allene and styrene substrates. Distortion/interaction analysis suggests that the distortion of CO₂ and Pd-C(allyl/benzyl) intermediates is the key factor that affects the reactivity of CO₂ insertion. The P-bound R substituents in pincer ligands can introduce significant steric repulsion in CO₂ insertion transition states, affecting the total distortion energy and thus changing the reactivity. These computational insights into ligand effects may be useful for designing efficient transition metal catalysts for formate salt and CO₂ utilization.

Conflicts of interest

There are no conflicts to declare.

Acknowledgements

This work was supported by the National Natural Science Foundation of China (21507025).

References

- J. Klankermayer, S. Wesselbaum, K. Beydoun and W. Leitner, *Angew. Chem., Int. Ed.*, 2016, **55**, 7296–7343.
- A. Behr, A. J. Vorholt, K. A. Ostrowski and T. Seidensticker, *Green Chem.*, 2014, **16**, 982–1006.
- J. C. Serrano-Ruiz, R. Luque and A. Sepulveda-Escribano, *Chem. Soc. Rev.*, 2011, **40**, 5266–5281.
- W. Leitner, *Angew. Chem., Int. Ed. Engl.*, 1995, **34**, 2207–2221.
- K. Sordakis, C. Tang, L. K. Vogt, H. Junge, P. J. Dyson, M. Beller and G. Laurenczy, *Chem. Rev.*, 2018, **118**, 372–433.
- J. Artz, T. E. Müller, K. Thenert, J. Kleinekorte, R. Meys, A. Sternberg, A. Bardow and W. Leitner, *Chem. Rev.*, 2018, **118**, 434–504.
- S. Enthaler, J. von Langermann and T. Schmidt, *Energy Environ. Sci.*, 2010, **3**, 1207–1217.
- G. Centi, E. A. Quadrelli and S. Perathoner, *Energy Environ. Sci.*, 2013, **6**, 1711–1731.
- M. Aresta, A. Dibenedetto and A. Angelini, *Chem. Rev.*, 2014, **114**, 1709–1742.
- A. K. Singh, S. Singh and A. Kumar, *Catal. Sci. Technol.*, 2016, **6**, 12–40.
- F. Jin, J. Yun, G. Li, A. Kishita, K. Tohji and H. Enomoto, *Green Chem.*, 2008, **10**, 612–615.
- R. Wolfel, N. Taccardi, A. Bosmann and P. Wasserscheid, *Green Chem.*, 2011, **13**, 2759–2763.
- W. Wang, M. Niu, Y. Hou, W. Wu, Z. Liu, Q. Liu, S. Ren and K. N. Marsh, *Green Chem.*, 2014, **16**, 2614–2618.
- Z. Zhang, J. Song and B. Han, *Chem. Rev.*, 2017, **117**, 6834–6880.
- L. T. Mika, E. Cséfalvay and Á. Németh, *Chem. Rev.*, 2018, **118**, 505–613.
- R. Noyori and S. Hashiguchi, *Acc. Chem. Res.*, 1997, **30**, 97–102.
- X. Wu and J. Xiao, *Chem. Commun.*, 2007, 2449–2466.
- A. Bartoszewicz, N. Ahlsten and B. Martin-Matute, *Chem. – Eur. J.*, 2013, **19**, 7274–7302.
- T. Morimoto and K. Kakiuchi, *Angew. Chem., Int. Ed.*, 2004, **43**, 5580–5588.
- L. Wu, Q. Liu, R. Jackstell and M. Beller, *Angew. Chem., Int. Ed.*, 2014, **53**, 6310–6320.
- J. Cao, Z.-J. Zheng, Z. Xu and L.-W. Xu, *Coord. Chem. Rev.*, 2017, **336**, 43–53.
- W. Ren, W. Chang, J. Dai, Y. Shi, J. Li and Y. Shi, *J. Am. Chem. Soc.*, 2016, **138**, 14864–14867.
- M.-C. Fu, R. Shang, W.-M. Cheng and Y. Fu, *ACS Catal.*, 2016, **6**, 2501–2505.
- J. Hou, M.-L. Yuan, J.-H. Xie and Q.-L. Zhou, *Green Chem.*, 2016, **18**, 2981–2984.
- W. Liu, W. Ren, J. Li, Y. Shi, W. Chang and Y. Shi, *Org. Lett.*, 2017, **19**, 1748–1751.
- M.-C. Fu, R. Shang, W.-M. Cheng and Y. Fu, *Chem. – Eur. J.*, 2017, **23**, 8818–8822.
- C. Zhu, J. Takaya and N. Iwasawa, *Org. Lett.*, 2015, **17**, 1814–1817.
- J. Takaya, K. Miyama, C. Zhu and N. Iwasawa, *Chem. Commun.*, 2017, **53**, 3982–3985.
- K. Huang, C.-L. Sun and Z.-J. Shi, *Chem. Soc. Rev.*, 2011, **40**, 2435–2452.
- Q. Liu, L. Wu, R. Jackstell and M. Beller, *Nat. Commun.*, 2015, **6**, 5933.
- S. Wang, G. Du and C. Xi, *Org. Biomol. Chem.*, 2016, **14**, 3666–3676.
- M. Börjesson, T. Moragas, D. Gallego and R. Martin, *ACS Catal.*, 2016, **6**, 6739–6749.
- J. Luo and I. Larrosa, *ChemSusChem*, 2017, **10**, 3317–3332.
- M. Hölscher, M. H. G. Prechtel and W. Leitner, *Chem. – Eur. J.*, 2007, **13**, 6636–6643.
- H.-W. Suh, T. J. Schmeier, N. Hazari, R. A. Kemp and M. K. Takase, *Organometallics*, 2012, **31**, 8225–8236.
- W. H. Bernskoetter and N. Hazari, *Eur. J. Inorg. Chem.*, 2013, **2013**, 4032–4041.
- C. Martin, S. Mallet-Ladeira, K. Miqueu, G. Bouhadir and D. Bourissou, *Organometallics*, 2014, **33**, 571–577.
- L. J. Murphy, H. Hollenhorst, R. McDonald, M. Ferguson, M. D. Lumsden and L. Turculet, *Organometallics*, 2017, **36**, 3709–3720.
- H.-W. Suh, L. M. Guard and N. Hazari, *Chem. Sci.*, 2014, **5**, 3859–3872.

- 40 X. Lv, L. Zhang, B. Sun, Z. Li, Y.-B. Wu and G. Lu, *Catal. Sci. Technol.*, 2017, 7, 3539–3545.
- 41 X. Lv, Y.-B. Wu and G. Lu, *Catal. Sci. Technol.*, 2017, 7, 5049–5054.
- 42 L. Dang, Z. Lin and T. B. Marder, *Organometallics*, 2010, 29, 917–927.
- 43 A. Uhe, M. Hölscher and W. Leitner, *Chem. – Eur. J.*, 2012, 18, 170–177.
- 44 R. Yuan and Z. Lin, *Organometallics*, 2014, 33, 7147–7156.
- 45 F. B. Sayyed and S. Sakaki, *Chem. Commun.*, 2014, 50, 13026–13029.
- 46 J. Jover and F. Maseras, *J. Org. Chem.*, 2014, 79, 11981–11987.
- 47 Q. Wang, C.-H. Guo, Y. Ren and H.-S. Wu, *J. Mol. Model.*, 2015, 21, 122.
- 48 M. Delarmelina, E. Marelli, J. W. de M. Carneiro, S. P. Nolan and M. Bühl, *Chem. – Eur. J.*, 2017, 23, 14954–14961.
- 49 F. M. Bickelhaupt and K. N. Houk, *Angew. Chem., Int. Ed.*, 2017, 56, 10070–10086.
- 50 M. J. Frisch, G. W. Trucks, H. B. Schlegel, G. E. Scuseria, M. A. Robb, J. R. Cheeseman, G. Scalmani, V. Barone, B. Mennucci, G. A. Petersson, H. Nakatsuji, M. Caricato, X. Li, H. P. Hratchian, A. F. Izmaylov, J. Bloino, G. Zheng, J. L. Sonnenberg, M. Hada, M. Ehara, K. Toyota, R. Fukuda, J. Hasegawa, M. Ishida, T. Nakajima, Y. Honda, O. Kitao, H. Nakai, T. Vreven, J. A. Montgomery, Jr., J. E. Peralta, F. Ogliaro, M. Bearpark, J. J. Heyd, E. Brothers, K. N. Kudin, V. N. Staroverov, R. Kobayashi, J. Normand, K. Raghavachari, A. Rendell, J. C. Burant, S. S. Iyengar, J. Tomasi, M. Cossi, N. Rega, J. M. Millam, M. Klene, J. E. Knox, J. B. Cross, V. Bakken, C. Adamo, J. Jaramillo, R. Gomperts, R. E. Stratmann, O. Yazyev, A. J. Austin, R. Cammi, C. Pomelli, J. W. Ochterski, R. L. Martin, K. Morokuma, V. G. Zakrzewski, G. A. Voth, P. Salvador, J. J. Dannenberg, S. Dapprich, A. D. Daniels, Ö. Farkas, J. B. Foresman, J. V. Ortiz, J. Cioslowski and D. J. Fox, *Gaussian 09, Revision D.01*, Gaussian, Inc., Wallingford, CT, 2009.
- 51 Y. Zhao and D. G. Truhlar, *Theor. Chem. Acc.*, 2008, 120, 215–241.
- 52 Y. Zhao and D. G. Truhlar, *Acc. Chem. Res.*, 2008, 41, 157–167.
- 53 A. V. Marenich, C. J. Cramer and D. G. Truhlar, *J. Phys. Chem. B*, 2009, 113, 6378–6396.
- 54 C. Y. Legault, *CYLVIEW, 1.0b*, Université de Sherbrooke, 2009.
- 55 Other conformers of CO₂ insertion transition states are less favorable due to larger distortion energies. See details in Fig. S3.†
- 56 The transition state for CO₂ reacting with benzylpalladium supported by the ^tBu-substituted-PGeP-pincer ligand cannot be computationally located. This is probably due to the considerable steric congestion around the Pd center which arises from the bulky ^tBu substituents.
- 57 The ligand electronic effects on CO₂ insertion reactivity are less significant. See details in Fig. S4 and S5.†